NATIONAL ENERGY TECHNOLOGY LABORATORY

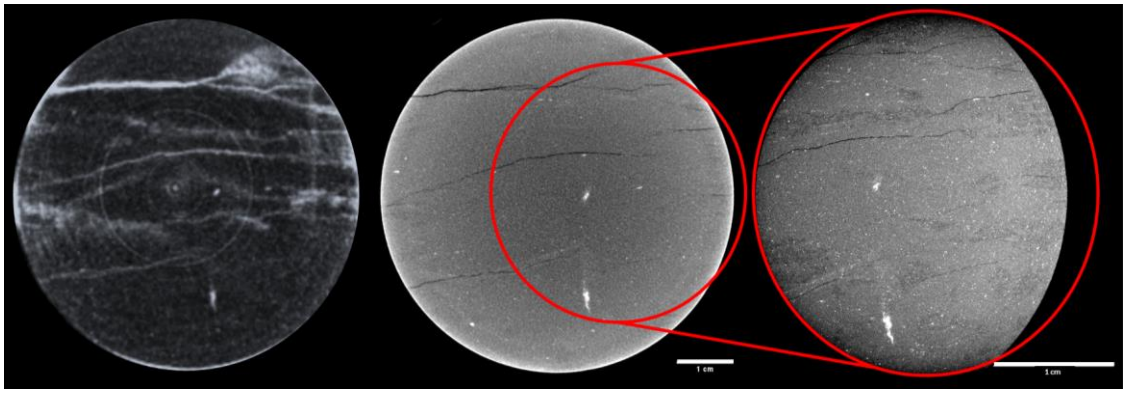

# Computed Tomography Scanning and Geophysical Measurements of State 16-2 Well in the Paradox Basin

29 September 2022

U.S. DEPARTMENT OF ENERGY | NATIONAL ENERGY TECHNOLOGY LABORATORY

**Office of Fossil Energy and Carbon Management**

DOE/NETL-2022/3736

# Disclaimer

This project was funded by the United States Department of Energy, National Energy Technology Laboratory, in part, through a site support contract. 

**Cover Illustration:** Xenon flooded sample 15 from a depth of 9,664.4 ft (left); white pixels indicate Xe flow pathways, DynaTOM micro CT image at 57.3 µm voxel resolution (center), and DynaTOM scan at 16 µm vowel resolution (right).

**Suggested Citation:** Paronish, T.; Mitchell, N.; Schmitt, R.; Brown, S.; Crandall, D.; Moore, J.; Edelman, E.; Esser, R.; McPherson, B. *Computed Tomography Scanning and Geophysical Measurements of State 16-2 Well in Paradox Basin;* DOE/NETL-2022/3736; NETL Technical Report Series; U.S. Department of Energy, National Energy Technology Laboratory: Morgantown, WV, 2022; p 44. DOI: https://doi.org/10.2172/1889878

**An electronic version of this report can be found at:**

https://netl.doe.gov/energy-analysis

https://edx.netl.doe.gov/ucr

The data in this report can be accessed from NETL's Energy Data eXchange (EDX) online system (https://edx.netl.doe.gov) using the following link: https://edx.netl.doe.gov/dataset/paradox-state-16-2.

# Computed Tomography Scanning and Geophysical Measurements of State 16-2 Well in the Paradox Basin

**Thomas Paronish[1,3], Natalie Mitchell[1,3], Rhiannon Schmitt[1,2], Sarah Brown[1,3], Dustin Crandall[1], Johnathan Moore[1,3], Eric Edelman[4], Rich Esser[4], Brian McPherson[4]**

**[1]National Energy Technology Laboratory, 3610 Collins Ferry Road, Morgantown, WV 26505**

**[2]Oak Ridge Institute for Science and Education (ORISE), 3610 Collins Ferry Road, Morgantown, WV 26505**

**[3]NETL Support Contractor, 3610 Collins Ferry Road, Morgantown, WV 26505**

**[4]University of Utah, Energy & Geosciences Institute, 423 Wakara Way, Salt Lake City, UT 84108**

---

**DOE/NETL-2022/3736**

29 September 2022

NETL Contacts:

Dustin Crandall, Principal Investigator

Christina Lopano and Eilis Rosenbaum, Technical Portfolio Leads

Bryan Morreale, Executive Director, Research & Innovation Center

This page intentionally left blank.

# Table of Contents

This page intentionally left blank.

# List of Figures

This page intentionally left blank.

# List of Tables

This page intentionally left blank.

# Acronyms, Abbreviations, and Symbols

| Term | Description |
|---|---|
| 2D | Two-dimensional |
| CT | Computed tomography |
| DOE | U.S. Department of Energy |
| EDX | NETL's Energy Data eXchange |
| MSCL | Multi-Sensor Core Logger |
| NETL | National Energy Technology Laboratory |
| RaSSCAL | Randolph Steady-State Core Analysis Laboratory |
| XRF | X-ray fluorescence |

# Acknowledgments

This work was completed at the National Energy Technology Laboratory with support from U.S. Department of Energy's (DOE) Office of Fossil Energy and Carbon Management. The authors wish to acknowledge Bryan Morreale and Ale Hakala for their technical support through the NETL Research & Innovation Center. The authors also wish to thank John Wimer (NETL Science & Technology Strategic Plans & Programs) and David Alleman (DOE Office of Resource Sustainability) for programmatic guidance, direction, and support.

The authors would like to thank Scott Workman and Bryan Tennant for data collection and technical support, and the University of Utah for providing the Paradox Basin cores for analyses. The cores were returned to the University of Utah, where they are currently stored.

## ABSTRACT

The computed tomography (CT) facilities and the Multi-Sensor Core Logger (MSCL) at the National Energy Technology Laboratory (NETL) in Morgantown, West Virginia, were used to characterize Paradox Basin core from Grand County, Utah.

The primary impetus of this work is a collaboration between the U.S. Department of Energy (DOE), the Utah Geological Survey, the University of Utah, and Zephyr Energy to characterize and make publicly available core information from the Cane Creek interval of the Paradox Basin. This stratigraphic well and the core data produced in this report will aid in understanding the structural complexities of the Cane Creek interval and its production potential. The resultant datasets are presented in this report and can be accessed from NETL's Energy Data eXchange (EDX) online system using the following link: https://edx.netl.doe.gov/dataset/paradox-state-16-2.

All equipment and techniques used were non-destructive, enabling future examinations and analyses to be performed on these cores. None of the equipment used was suitable for direct visualization of the pore space in the fine-grained structures studied; fractures, discontinuities, and millimeter-scale features were readily detectable with the methods tested. Imaging with the NETL medical CT scanner was performed on the entire core. Targeted higher resolution CT scanning of select sections was performed with NETL's industrial and micro CT scanner. Qualitative analysis of the medical CT images, coupled with X-ray fluorescence (XRF), P-wave, and magnetic susceptibility measurements from the MSCL were useful in identifying zones of interest for more detailed analysis. The ability to quickly identify key areas for more detailed study with higher resolution will save time and resources in future studies. The combination of methods used provides a multi-scale analysis the core; the resulting macro and micro descriptions are relevant to many subsurface energy related examinations traditionally performed at NETL.

# 1. INTRODUCTION

Evaluation of core data from ongoing and emerging unconventional reservoirs has long been a priority of the U.S. Department of Energy's (DOE) National Energy Technology Laboratory (NETL). In fulfillment of this mission, the goal of this report is to characterize and disseminate data from the State 16-2 well, a stratigraphic test well in Southwest Utah, drilled to explore the structural complexity and production potential of the Crane Creek resource play and aid in developing a strategy to produce from this emerging play. This report builds on the techniques of previous core characterization technical reports and aims to meet the growing demand for high-quality and comprehensive lithological data.

The primary objective for this study was to characterize core from an unconventional reservoir in a growing and emerging field, utilizing methods not available to most researchers. The computed tomography (CT) and the Multi-Sensor Core Logger (MSCL) at NETL in Morgantown, WV, provides a means to characterize the well and disseminate the data to the public in several formats; including this report and through NETL's Energy Data eXchange (EDX). While the data presented in this report is meant to assist other researchers more detailed analyses, additional analyses on the complex interplay of pressure and fracture transmissivity in subcores from the Cane Creek formation have been described elsewhere (Paronish et al., 2021).

## 1.1 SITE BACKGROUND

Located in the southeastern region of Utah, the Paradox Basin has a legacy of natural resource production of oil, natural gas, helium, and potash. A hydrocarbon resource study by Whidden et al. (2012) calculated the total oil present in the Cane Creek portion of the Paradox Basin to be 215 million barrels, and in excess of 471 million barrels in the extended region (Whidden et al., 2012). The surrounding clastic intervals have also shown signs of economic hydrocarbon reservoir potential. The Paradox Formation contains 29 halite cycles, with the Cane Creek interval sitting between cycles 21 and 22. The halite provides a hydraulic seal that prevents hydrocarbons from escaping from the bounded intervals. However, the plastic deformation of the halite over extended time, has fractured the stiff reservoir rock. Due to the complexity of the halite cycles, a limited number of companies have attempted to drill and produce from the Cane Creek.

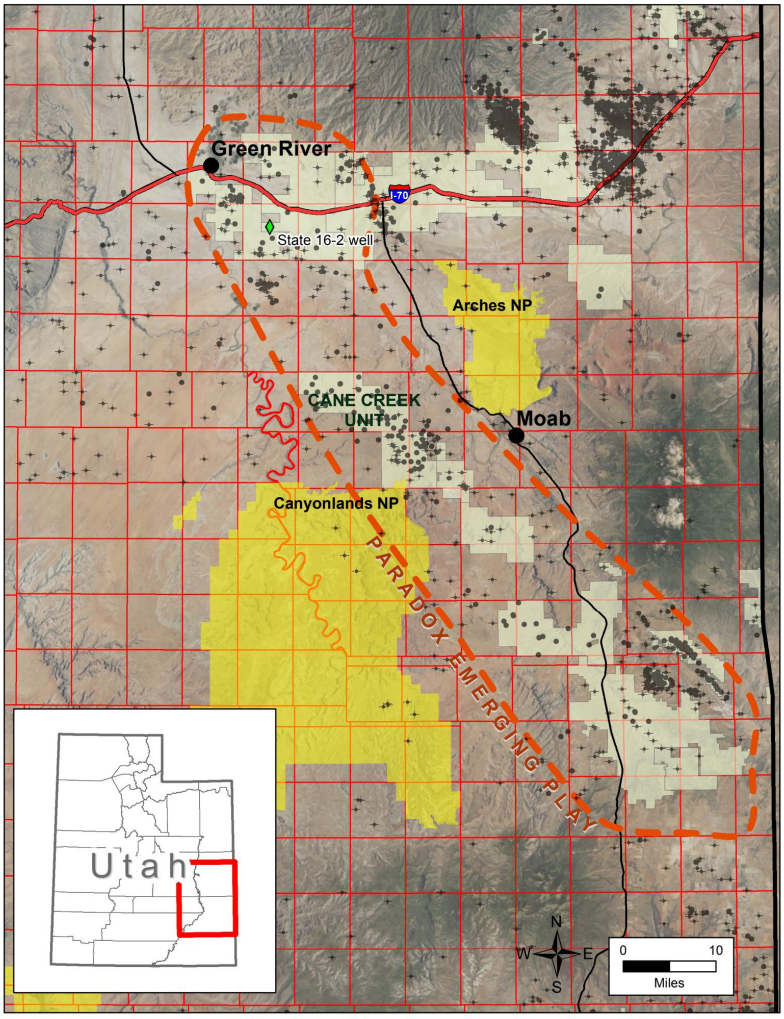


**Figure 1: Map of the Paradox Play in southeastern Utah; the green diamond represents the State 16-2 well location.**

Including the recent horizontal well drilled for this project, 38 wells have been drilled into the Cane Creek and 27, all horizontal, have been deemed producers. Figure 1 defines the legacy production of the Cane Creek, land ownership, and other associated project details. The producing wells have almost all been drilled in the central Cane Creek interval. With the successful drilling of the project well in the north Cane Creek, it is anticipated that the understanding gained from the successful central Cane Creek wells and the application of the testing and reservoir evaluation work performed within this project will enable more efficient access to the more than 206 million barrels remaining within the interval.

The CT imaging, characterization, and permeability work performed on the extracted core from this well are being used to understand how the fluids are traveling within the rock matrix and fractures. This work is also being coupled with simulations, field measurements, and external laboratory testing to understand how the existing fracture network within the Cane Creek may be utilized to enhance the hydrocarbon production while keeping the bounding halite layer stable.

## 2. CORE PHOTOGRAPHS

Core photographs are presented to complement the CT imaging and core logging.

**State 16-2 Core:**

**9,638–9,652 ft** **9,652–9,666 ft**

**9,666–9,681 ft** **9,681–9,696 ft**

**Figure 2: State 16-2 core photographs from 9,638 to 9,696 ft.**

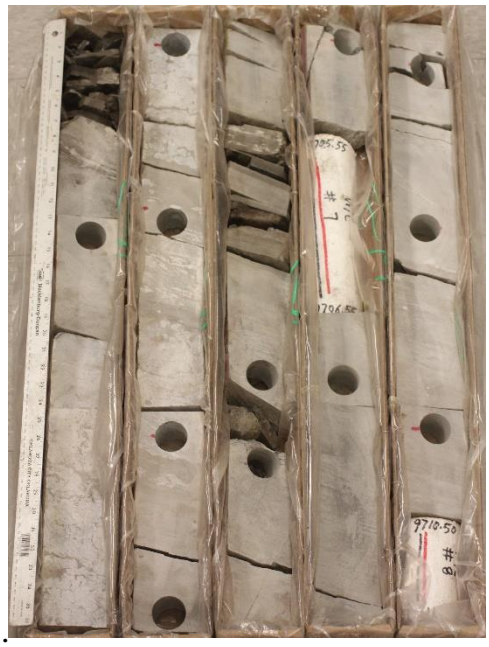

**9,696–9,711 ft**

**9,711–9,726 ft**

**9,726–9,741 ft**

**9,741–9,748 ft**

**Figure 3: State 16-2 core photographs from 9,696 to 9,748 ft.**

# 3. DATA ACQUISITION AND METHODOLOGY

The core was evaluated using CT scanning, MSCL, and X-ray fluorescence (XRF) spectrometry.

## 3.1 MEDICAL CT SCANNING

Core scale CT scanning was conducted with a Toshiba® Aquilion TSX-101A/R medical scanner as shown in Figure 4. The medical CT scanner generates images with a resolution in the millimeter range, with scans having voxel resolutions of 0.43 x 0.43 mm in the XY plane and 0.50 mm along the core axis. The scans were conducted at a voltage of 135 kV and at a current of 200 mA. Subsequent processing and combining of stacks were performed to create three-dimensional volumetric representations of the cores and a two-dimensional (2D) cross-section through the middle of the core samples using ImageJ (Rasband, 2018). The variation in greyscale values observed in the CT images indicates changes in the CT number obtained from the CT scans, which is directly proportional to changes in the attenuation and density of the scanned rock. Darker regions are less dense. As can be seen in Figure 11 through Figure 20, filled fractures, open fractures, and changes in bedding structure can all be resolved via careful examination of the CT images. While the medical CT scanner was not used for detailed characterization in this study, it allowed for non-destructive bulk characterization of the core.

**Figure 4: Toshiba® Aquilion™ Multislice Helical CT Scanner at the NETL used for core analysis.**

## 3.2 INDUSTRIAL CT SCANNING

High-resolution CT scans were performed on intervals of interest using the North Star Imagining Inc. M-5000® Industrial CT System shown in Figure 5. The system is used to obtain higher resolution scans, resolving some unclear features from the medical scans.

The scans were performed at varying voltages and currents to provide a balance between resolution and a sufficient sample penetration for each sample. Scans consisted of 1,440 radiographs, or at every 0.25°; radiographs were comprised of 10 images averaged with a 5 second acquisition for each image to ensure sufficient image contrast.

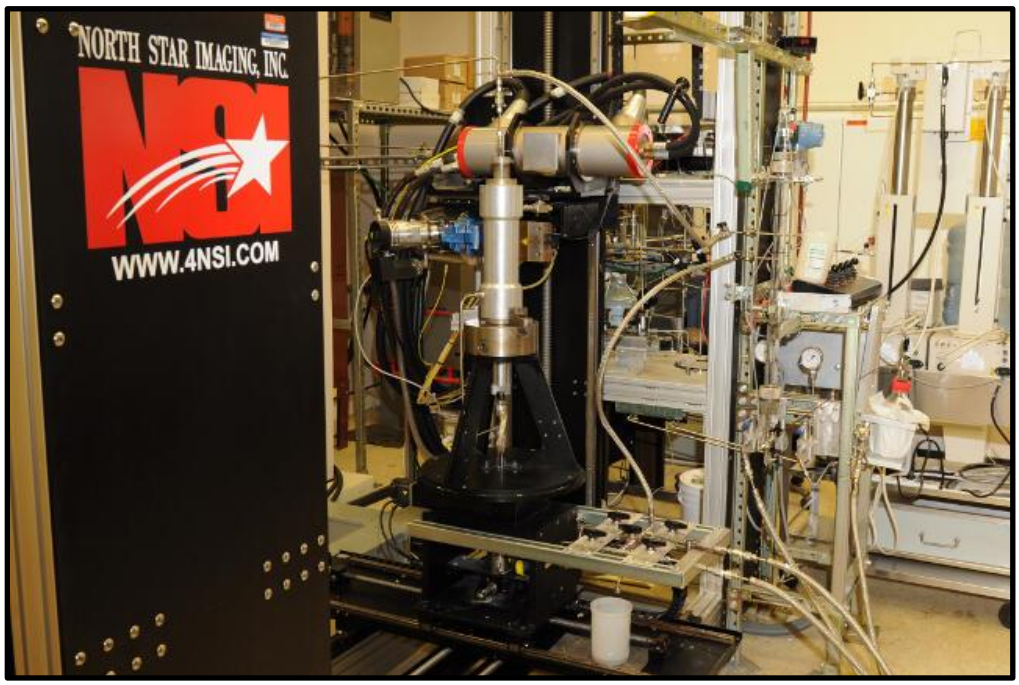


**Figure 5: North Star Imaging Inc. M-5000 ® Industrial CT Scanner at NETL used for core analysis.**

## 3.3 MICRO-CT SCANNING

Micro-CT scanning was performed using two scanners, a ZEISS Xradia MicroXCT-*400* (Xradia) scanner and a Tescan DynaTOM micro-CT (Dynatom) scanner. The Xradia system has the highest resolution of the scanners at NETL and scans samples sized from sub-mm to 25 mm. The Dynatom performs both dynamic and static imaging and has the ability to scan both sub-mm to cm-scale samples (Figure 6). Both scanners provide detailed image data that can be used to infer porosity, mineralogy, and structure.


**Figure 6: Tescan DynaTOM micro-CT scanner used for high-resolution CT images at NETL used for core analysis.**

## 3.4 STEADY STATE PERMEABILITY

The Randolph Steady-State Core Analysis Laboratory (RaSSCAL) is a custom-made permeability measuring device designed to measure low permeability samples with a steady differential pressure and gas flow across a tight core. A schematic of the RaSSCAL can be seen in Figure 7.

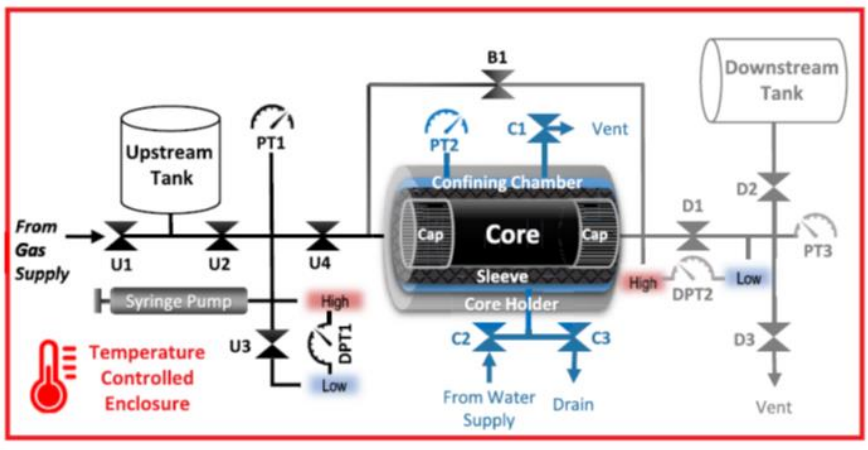


**Figure 7: Schematic for the RaSSCAL.**

The system uses a Hassler style core holder with a large volume gas cylinder on the upstream and downstream side of the system. These large volumes allow the system to maintain a consistent pressure gradient across the sample for long-term testing. The upstream pressure setpoint is at least 1 psi higher than the downstream to induce flow. A small segment of line of known volume downstream of the core is connected to a differential pressure gauge and a pneumatically actuated valve. When the downstream segment reaches 0.45 psi, the valve opens, and the gas is purged to equilibrate to downstream pressure. This process is repeated until the integrated time to reach the 0.45 psi threshold is consistent at which time permeability can be calculated (Figure 8). Further information on the calculation methods used to directly determine the permeability is given by Hannon et al. (2019).

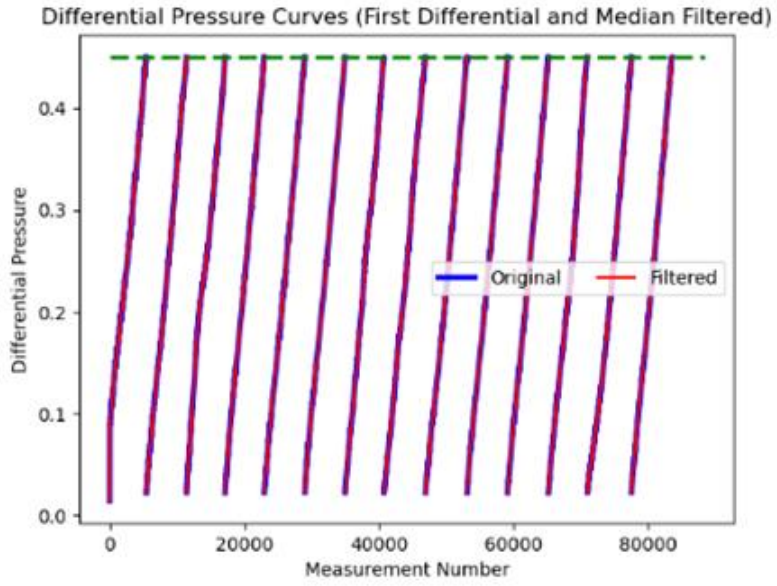


**Figure 8: Differential pressure curves from steady state measurements.**

## 3.5 CORE LOGGING

Geophysical measurements of P-wave travel time, magnetic susceptibility, and attenuated gamma counts were obtained with a Geotek® Multi-Sensor Core Logging system on competent sections of the core (Figures 26 and 27). Additionally, the system was used to measure bulk elemental chemistry with a built-in, portable XRF spectrometer.

The compiled core logs were scaled to fit on single pages for rapid review of the combined data from the medical CT scans and XRF readings. Core scale CT scanning was done with a medical Toshiba® Aquilion TSX-101A/R medical scanner.

### 3.5.1 Magnetic Susceptibility

Magnetic susceptibility is a measure of the degree of magnetization in a sample. The sample is exposed to an external magnetic field and magnetic susceptibility is the measured magnetic response to that field:

$$J = kH$$

Where, $J$ is the magnetic response (per unit volume), $k$ is volume susceptibility, and $H$ is an external magnetic field. The measurement unit is dimensionless (abbreviated simply as SI). All materials have magnetic susceptibility. Positive values of magnetic susceptibility indicate that materials are paramagnetic and occur in rocks that are the majority ferromagnetic, ferrimagnetic, or antimagnetic (iron bearing) materials. Negative values of magnetic susceptibility indicate that materials are diamagnetic and they occur in rocks dominated by non-iron material (i.e., calcite or quartz). Table 1 lists examples of common magnetic susceptibility ranges (Hunts et al., 1995).

Magnetic susceptibility is measured using the Bartington point sensor, where a 1-cm diameter, low intensity (8.0 A/m RMS), non-sensitive, alternating magnetic field (2 kHz) is generated for 10 seconds. To minimize any potential drift in the oscillating field the point sensor is zeroed at the beginning and end of the sample, as well as, after every fifth measurement. The point sensor due to the small field, is limited in whole core measurements, and additionally is temperature dependent (Geotek Ltd. Multi-Sensor Core Logger Manual, Version 05-10).

**Table 1: Magnetic Susceptibility Values for Common Minerals (Hunts et al., 1995)**

| Mineral | X (*10-6) SI |
|---|---|
| Water | 9 |
| Calcite | -7.5 to -39 |
| Halite, Gypsum | -10 to -60 |
| Illite, Montmorillonite | 330 to 410 |
| Pyrite | 5 to 3,500 |
| Haematite | 500 to 40,000 |
| Magnetite | 1,000,000 to 5,700,000 |

### 3.5.2 P-wave Velocity

P-wave velocity measurements are performed to measure the acoustic impedance of a geologic sample with compressional waves. Acoustic impedance is a measure of how well a material transmits vibrations, which is directly proportional to density and material consolidation. An example of a material that has a low acoustic impedance would be air, with a wave speed of 330 m/s, whereas granite would have high acoustic impedance, with a wave speed of >5,000 m/s. These measurements can be proxies for seismic reflection coefficients and can be translated to field use when doing seismic surveys.

The software associated with the MSCL measures the travel time of the pulse with a resolution of 50 ns. The absolute accuracy of the instrument measurements is $\pm$ 3 m/s with a resolution of 1.5 m/s (Geotek Ltd. Multi-Sensor Core Logger Manual, Version 05-10; Geotek Ltd., 2010).

### 3.5.3 Gamma Density

Gamma density is acquired by subjecting the sample to gamma radiation and then measuring the attenuation of that radiation. The attenuation is directly proportional to the density of the sample and is acquired by measuring the difference between radiation energy at the emission source and after it passes through the sample. Specifically, the MSCL software calculates the bulk density, $\rho$, by using the following equation:

$$\rho = \left(\frac{1}{\mu d}\right) \ln\left(\frac{I_o}{I}\right)$$

Where $\mu$ is the Compton attenuation coefficient, $d$ is the sample thickness, $I_o$ is the source intensity, and $I$ is the measured intensity.

## 3.6 XRF SPECTROMETRY

In addition to the geophysical measurements, a portable handheld Innov-X® X-Ray Fluorescence Spectrometer was used to measure relative elemental abundances of aggregated "light elements" up to and including sodium, and various heavy elements which were measured individually (Figure 9). Elemental abundances are reported in ppm relative to the total elemental composition (i.e., the total XRF counts).

The XRF spectrometer measures elemental abundances by subjecting the sample to X-ray photons. The high energy of the photons displaces inner orbital electrons in the respective elements. The vacancies in the lower orbitals cause outer orbital electrons to "fall" into lower orbits to satisfy the disturbed electron configuration. The substitution into lower orbitals causes a release of a secondary X-ray photon, which has an energy associated with a specific element. These relative and element specific energy emissions can then be used to determine bulk elemental composition.

The "Mining-Plus Suite" was run at 10 cm resolution for 60 s exposure time analysis. The Mining-Plus Suite utilizes a 2-beam analysis that resolves major (Mg, Al, Si, P, S, Cl, Fe, K, Ca, and Ti), minor (V, Cu, Ni, Cr, Mn, and Pb), and trace elements (Co, Zn, As, Zr, Mo, Ag, Cd, Sn, Sb, Hf, W, and Bi). The system also resolves an aggregated "light element" (H to Na).

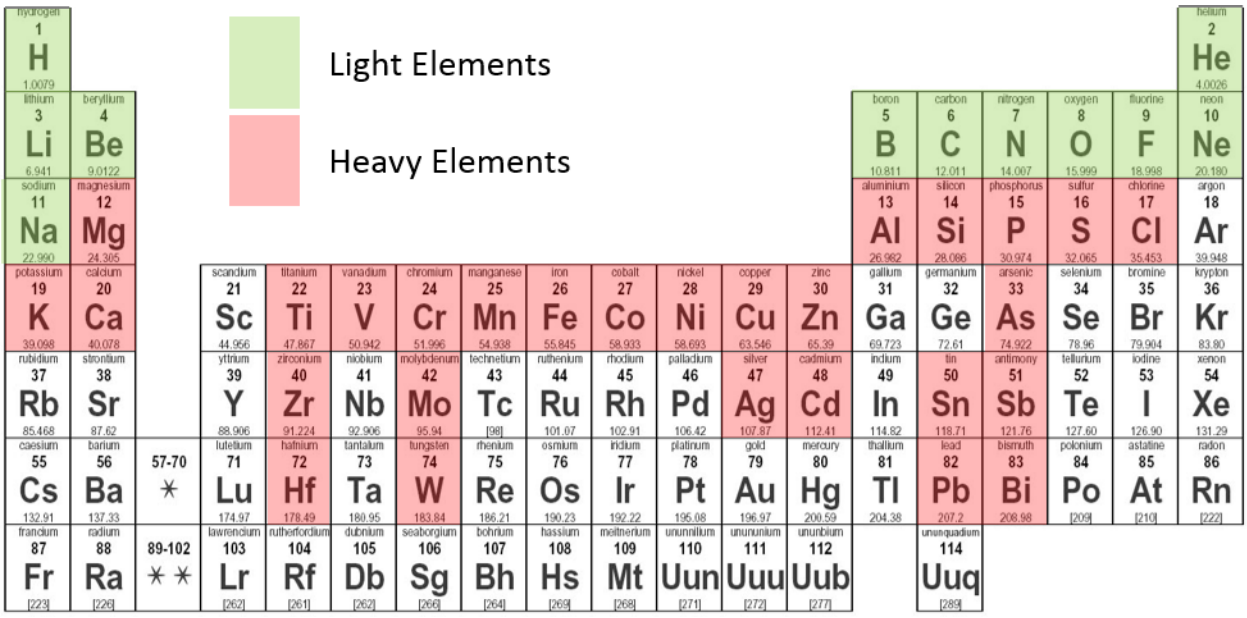


**Figure 9: Periodic table showing elements measurable by the Innov-X® X-Ray Fluorescence Spectrometer using the Mining-Plus and Soil modes (shaded).**

## 3.7 DATA COMPILATION

Strater® by Golden Software® was used to compile the medical CT data into a series of logs. The data used to generate these logs can be accessed from NETL's EDX online system using the following link: https://edx.netl.doe.gov/dataset/paradox-state-16-2.

# 4. RESULTS

Processed 2D slices of the medical CT scans through the cores are shown in this section.

## 4.1 MEDICAL CT SCANS

As was discussed previously, the variation in greyscale values observed in the medical CT images indicates changes in the CT number obtained, which is directly proportional to changes in the attenuation and density of the scanned rock (i.e., darker regions are less dense). Detailed information in logbooks and photographs of the core was used to confirm the locations of missing core and depths.

### 4.1.1 XZ Planes

A 2D image through the center of each core can be found in Figure 11 through Figure 20. These are referred to as XZ planes with the coordinates that are shown in Figure 10. There is a 2 cm scale bar shown in these images; the retrieved core has a diameter of 2 in. (5.08 cm) for reference. The labels below each 2D XZ plane in Figure 11 through Figure 20 are the depth range of each boxed core section; the full range of core lengths shown in each figure is listed in the figure captions. The greyscale range was maintained for all core CT images.

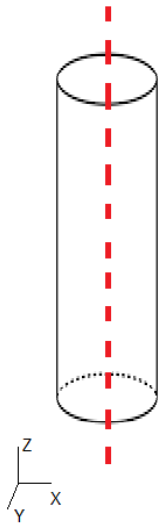


**Figure 10: Schematic of the XZ isolated plane through the vertical center of the medical CT scans.**

## State 16-2:

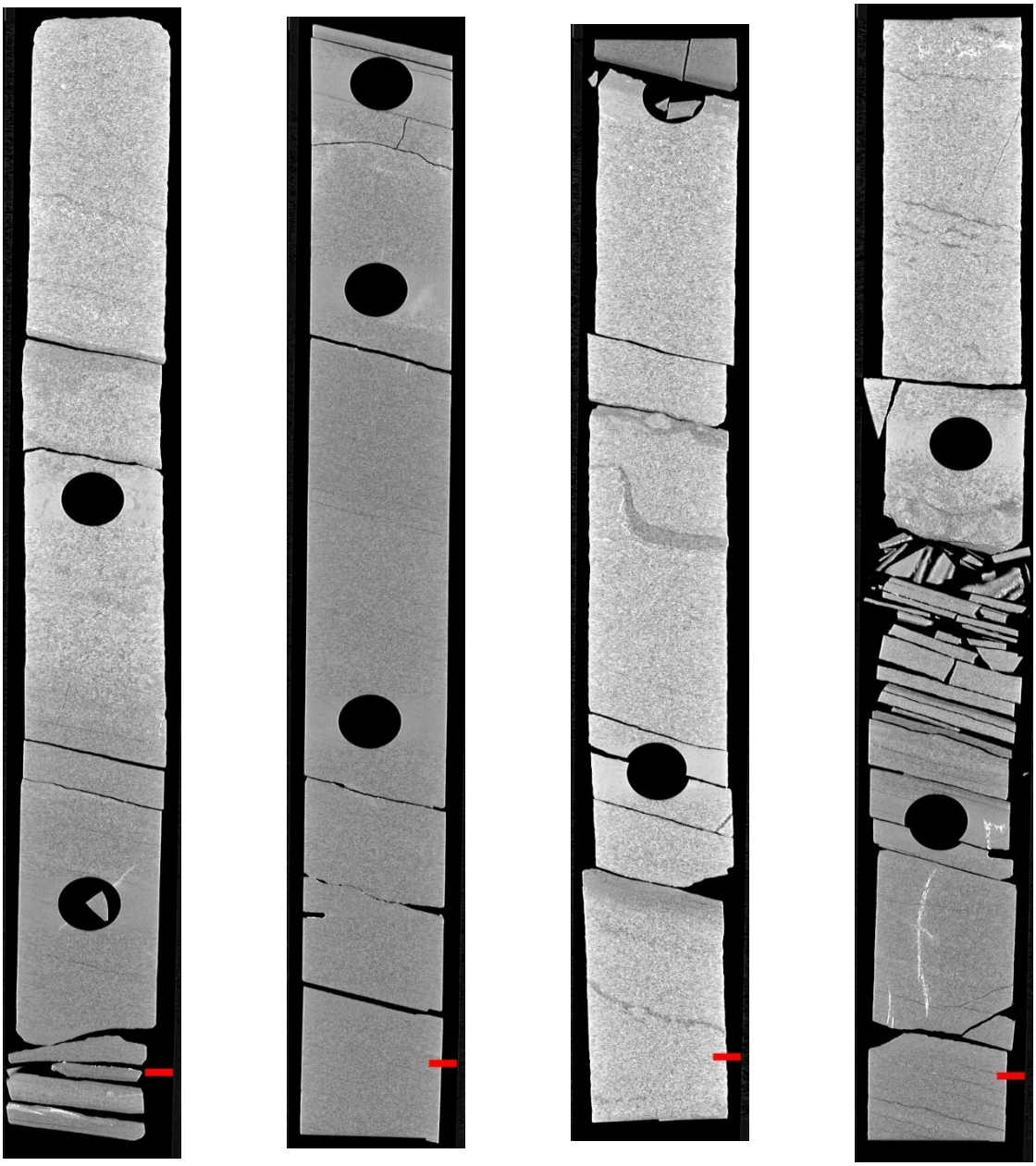

9,638–9,641 ft | 9,641–9,644 ft | 9,644–9,647 ft | 9,647–9,650 ft

**Figure 11: 2D isolated planes through the medical CT scans of the State 16-2 from 9,638 to 9,650 ft.**

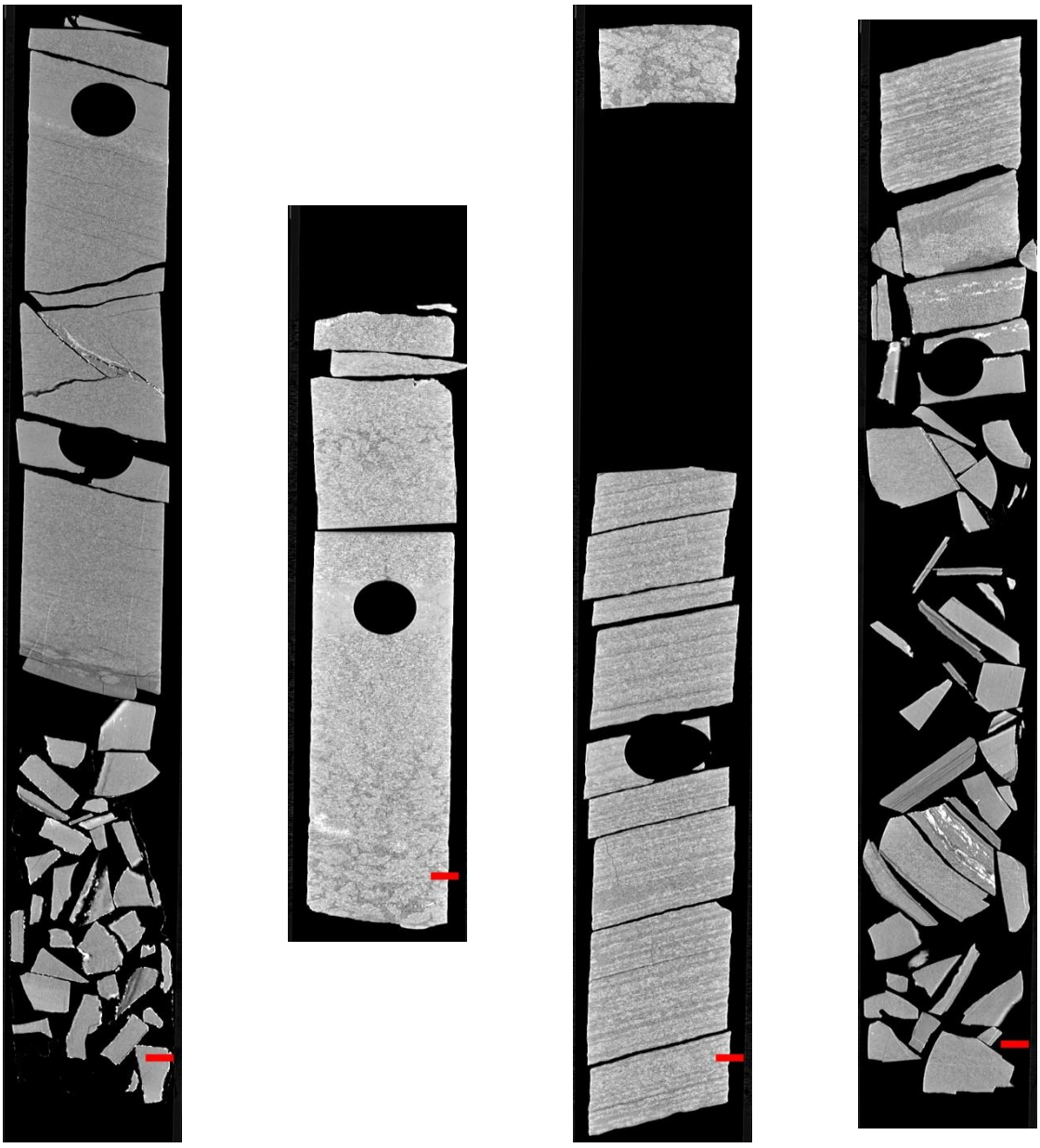

9,650–9,652 ft 9,652–9,654 ft 9,654–9,657 ft 9,657–9,660 ft

**Figure 12: 2D isolated planes through the medical CT scans of the State 16-2 from 9,650 to 9,660 ft.**

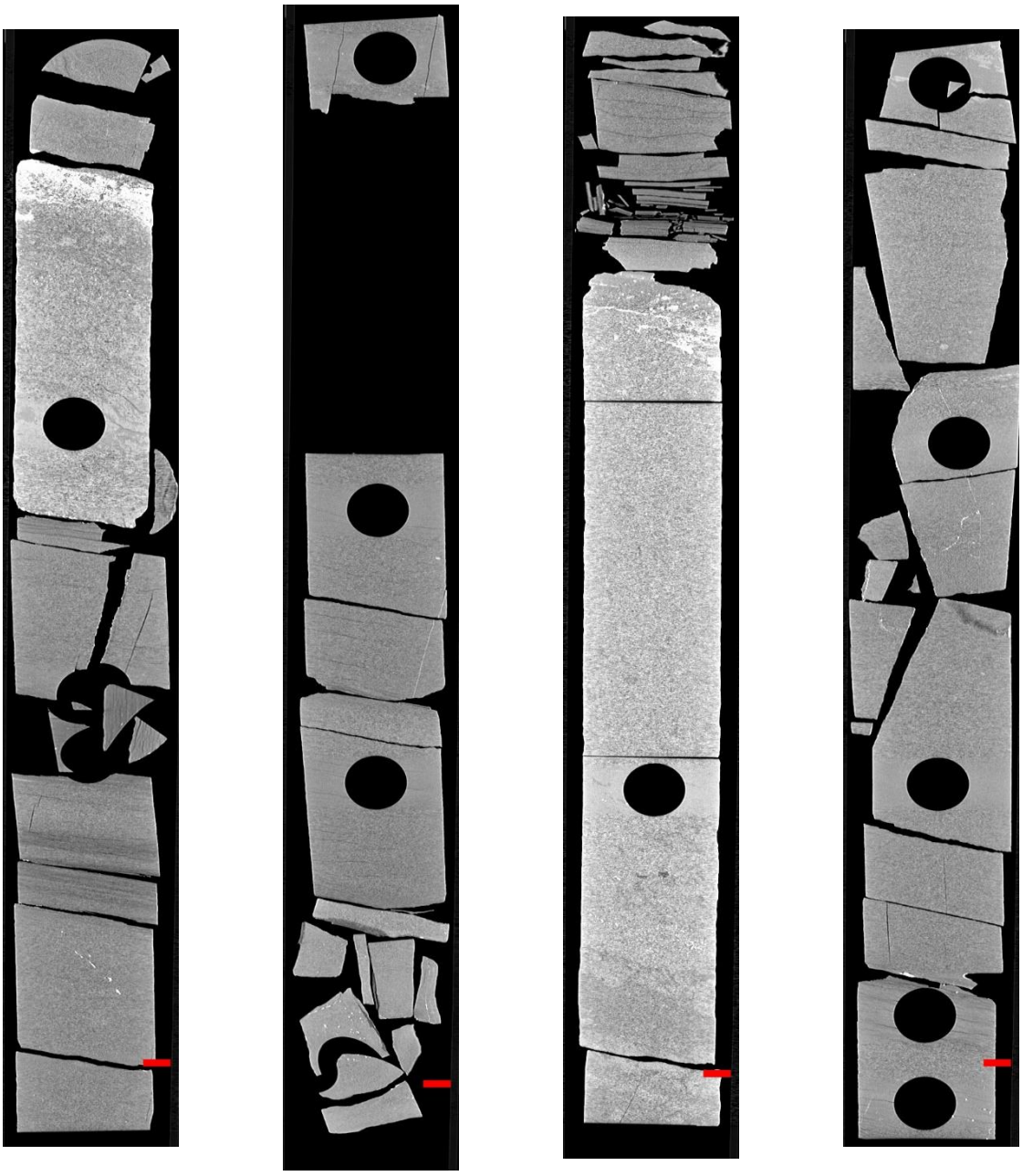

9,660–9,663 ft | 9,663–9,666 ft | 9,666–9,669 ft | 9,669–9,672 ft

**Figure 13: 2D isolated planes through the medical CT scans of the State 16-2 from 9,660 to 9,672 ft.**

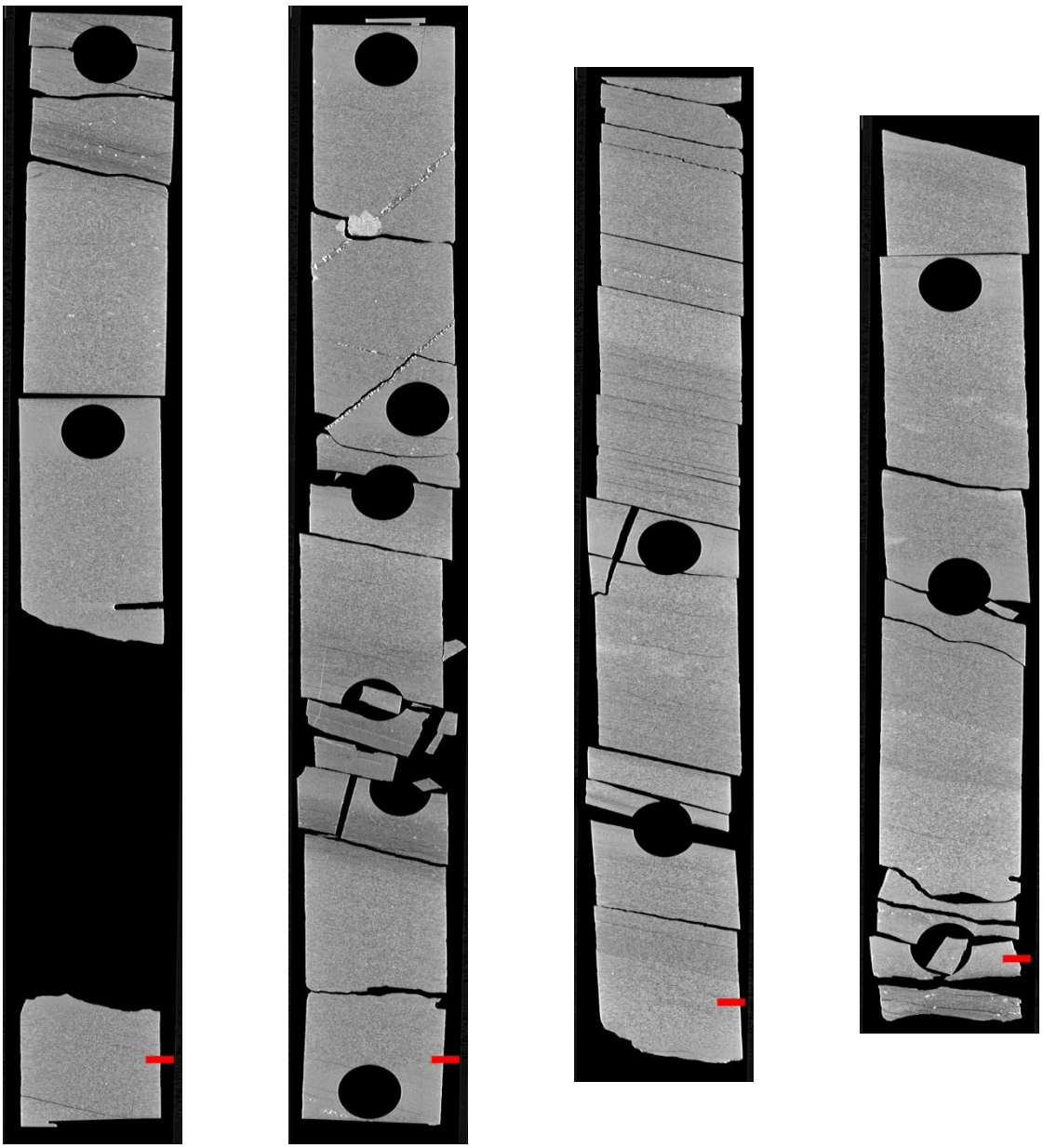

9,672–9,675 ft 9,675–9,678 ft 9,678–9,681 ft 9,681–9,684 ft

**Figure 14: 2D isolated planes through the medical CT scans of the State 16-2 from 9,672 to 9,684 ft.**

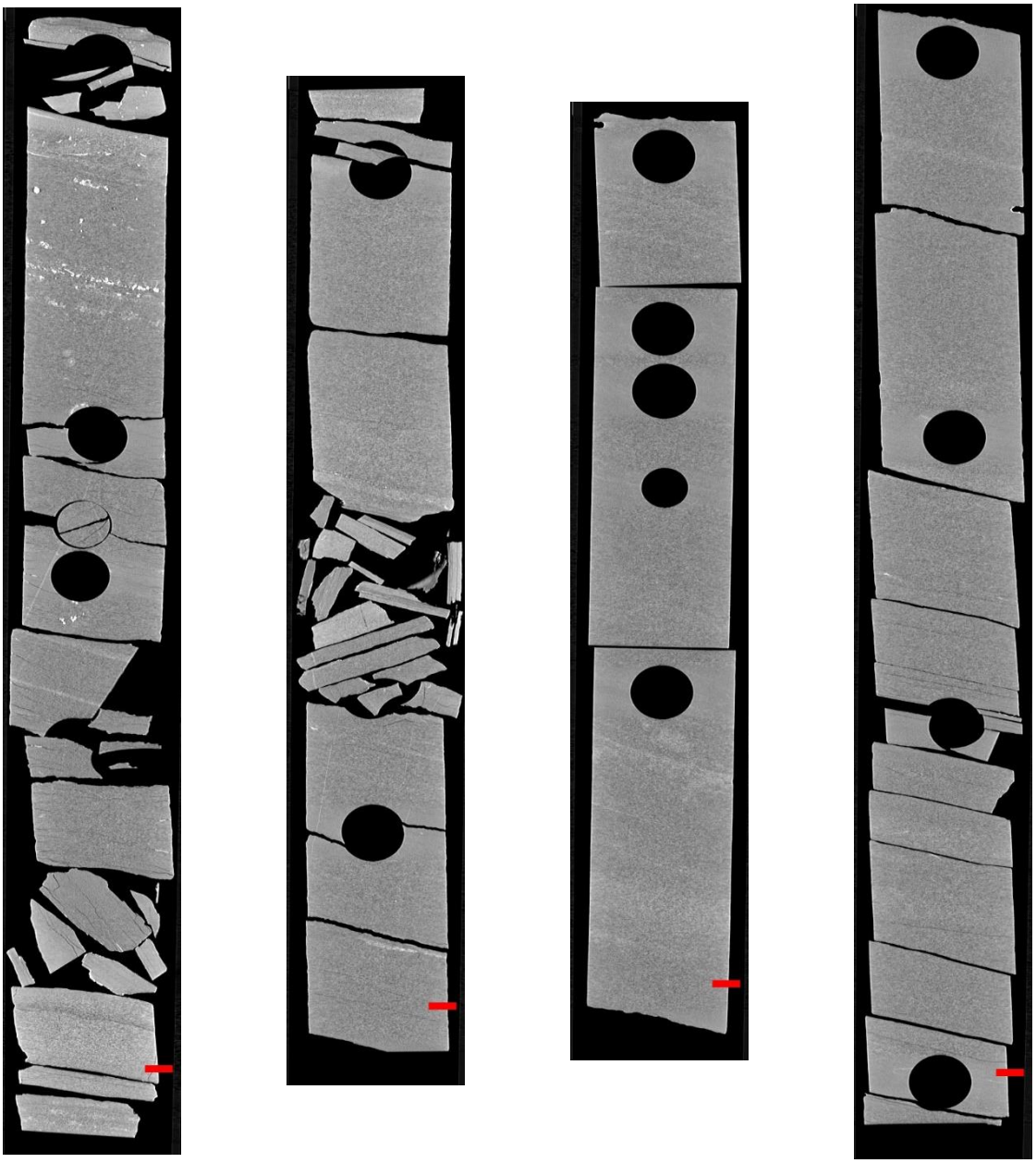

9,684–9,687 ft 9,687–9,690 ft 9,690–9,693 ft 9,693–9,696 ft

**Figure 15: 2D isolated planes through the medical CT scans of the State 16-2 from 9,684 to 9,696 ft.**

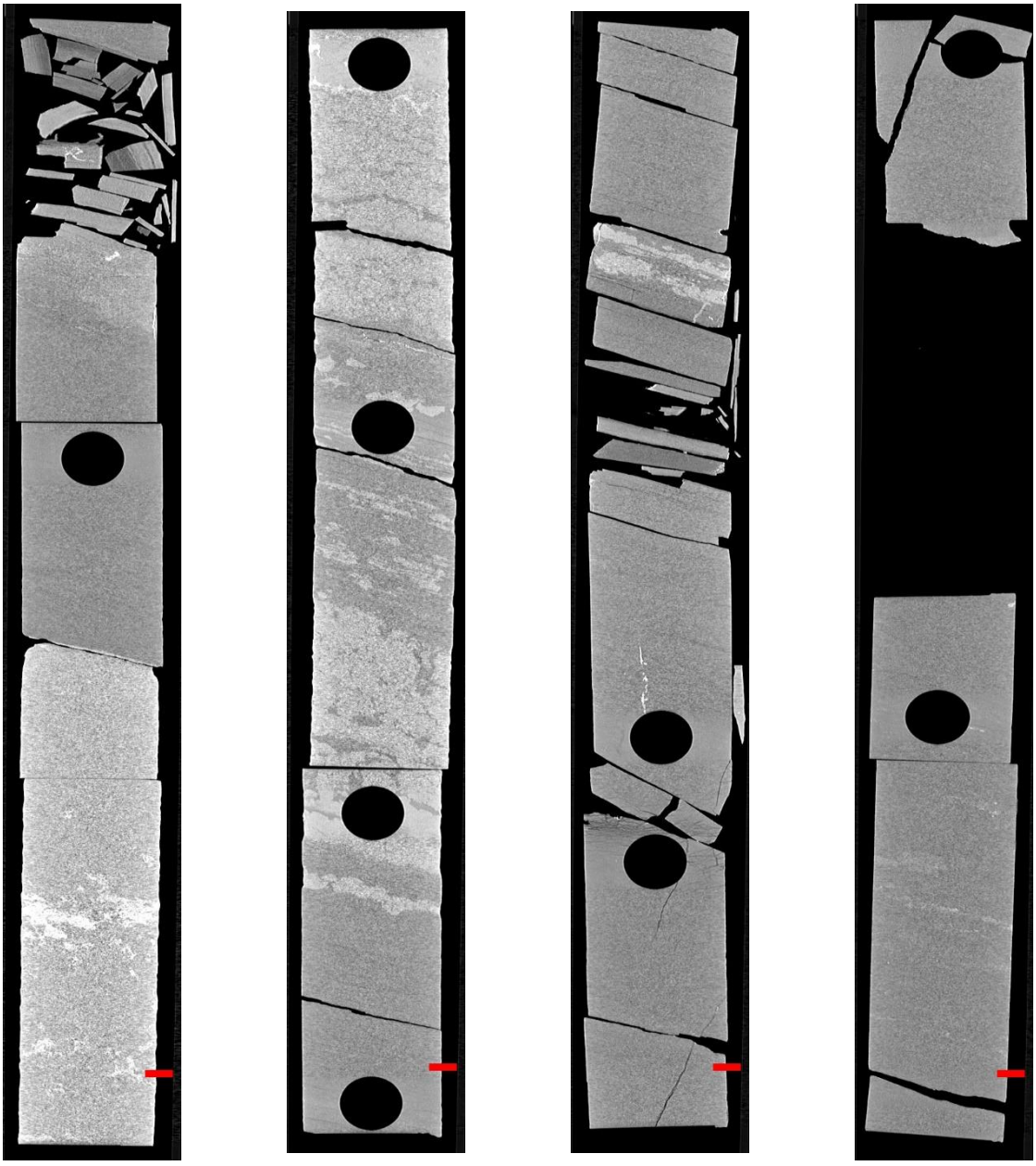

9,696–9,699 ft 9,699–9,702 ft 9,702–9,705 ft 9,705–9,708 ft

**Figure 16: 2D isolated planes through the medical CT scans of the State 16-2 from 9,696 to 9,708 ft.**

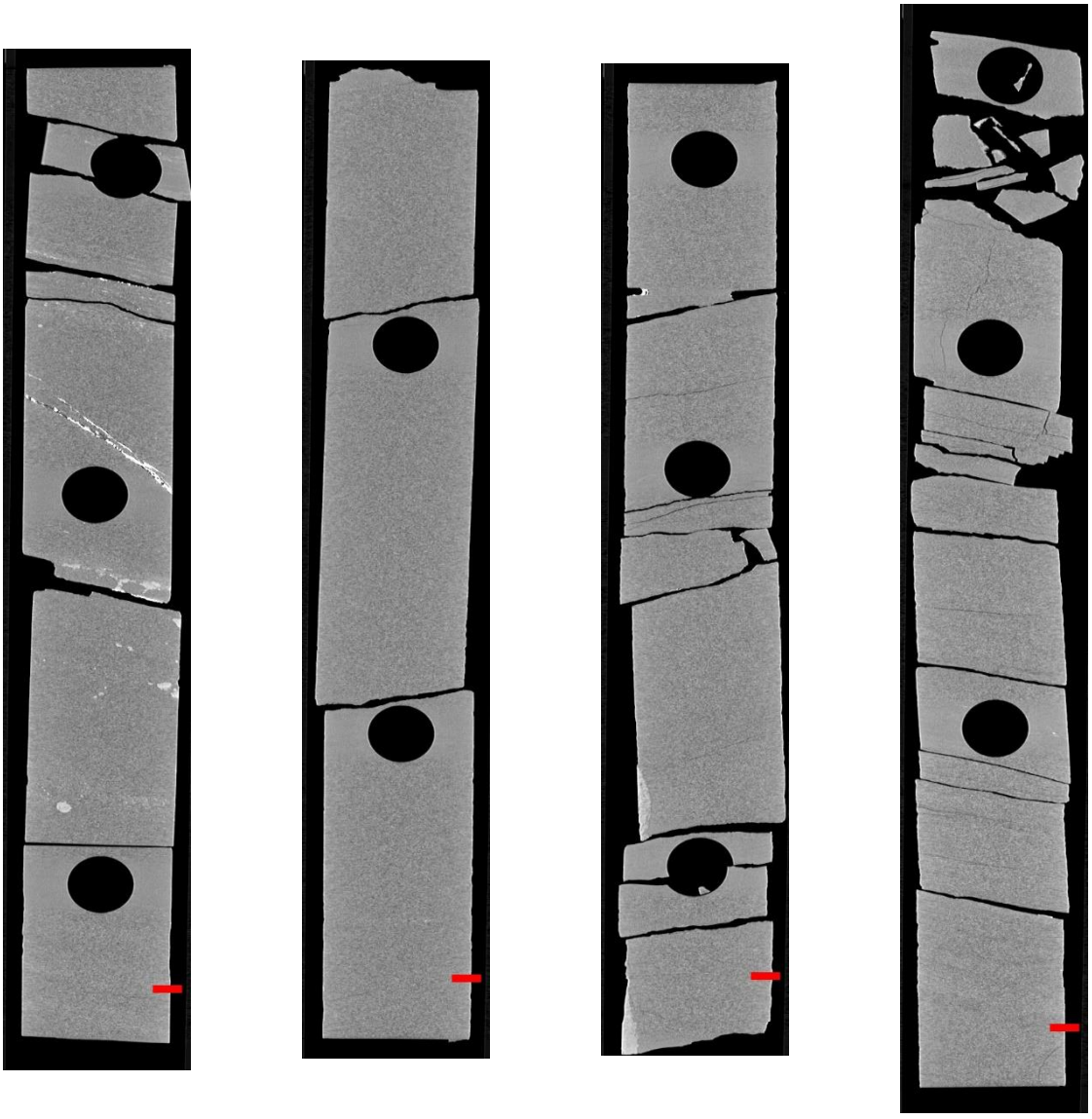

**9,708–9,711 ft** **9,711–9,714 ft** **9,714–9,717 ft** **9,717–9,720 ft**

**Figure 17: 2D isolated planes through the medical CT scans of the State 16-2 from 9,708 to 9,720 ft.**

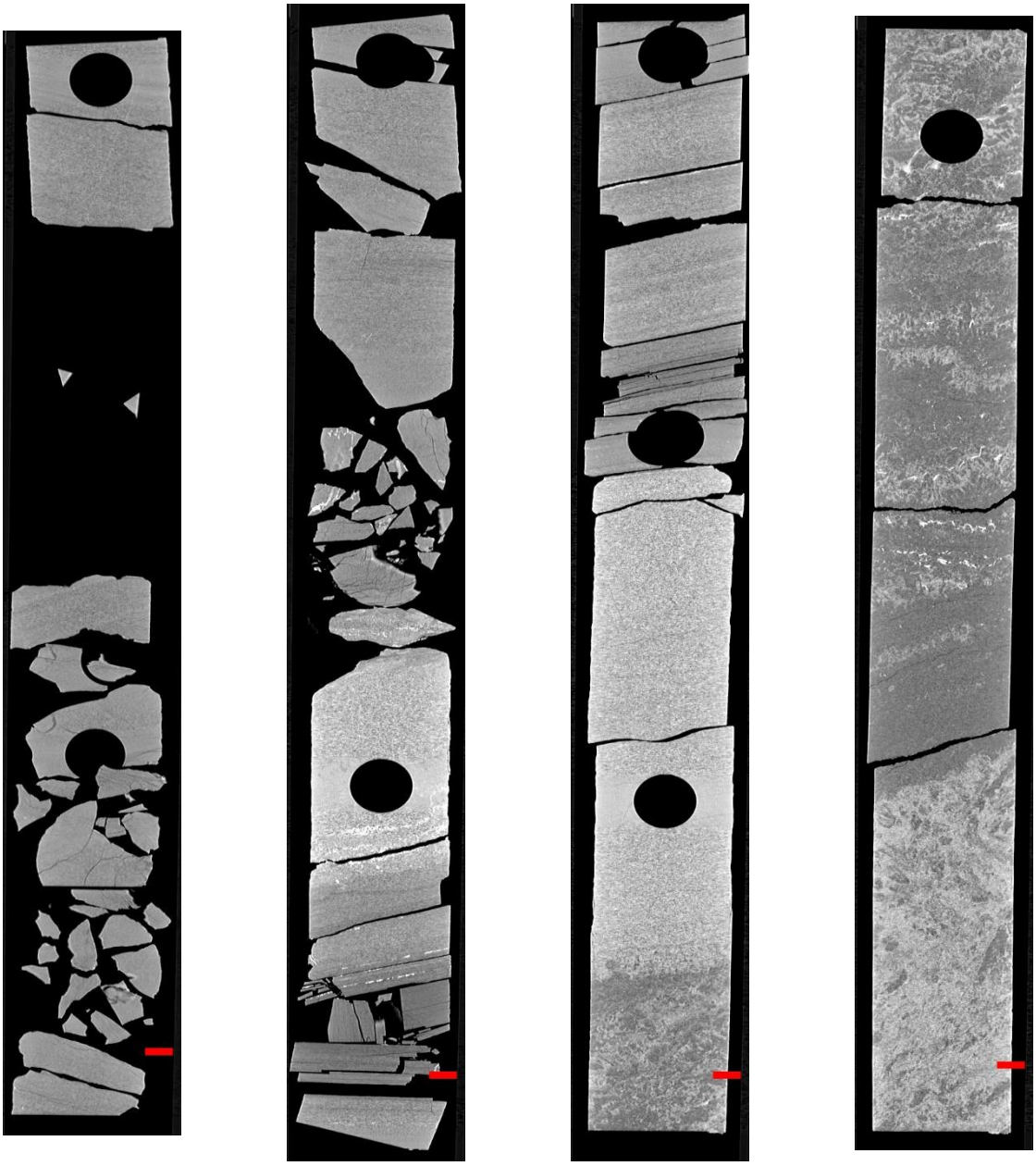

9,720–9,723 ft 9,723–9,726 ft 9,726–9,729 ft 9,729–9,732 ft

**Figure 18: 2D isolated planes through the medical CT scans of the State 16-2 from 9,720 to 9,732 ft.**

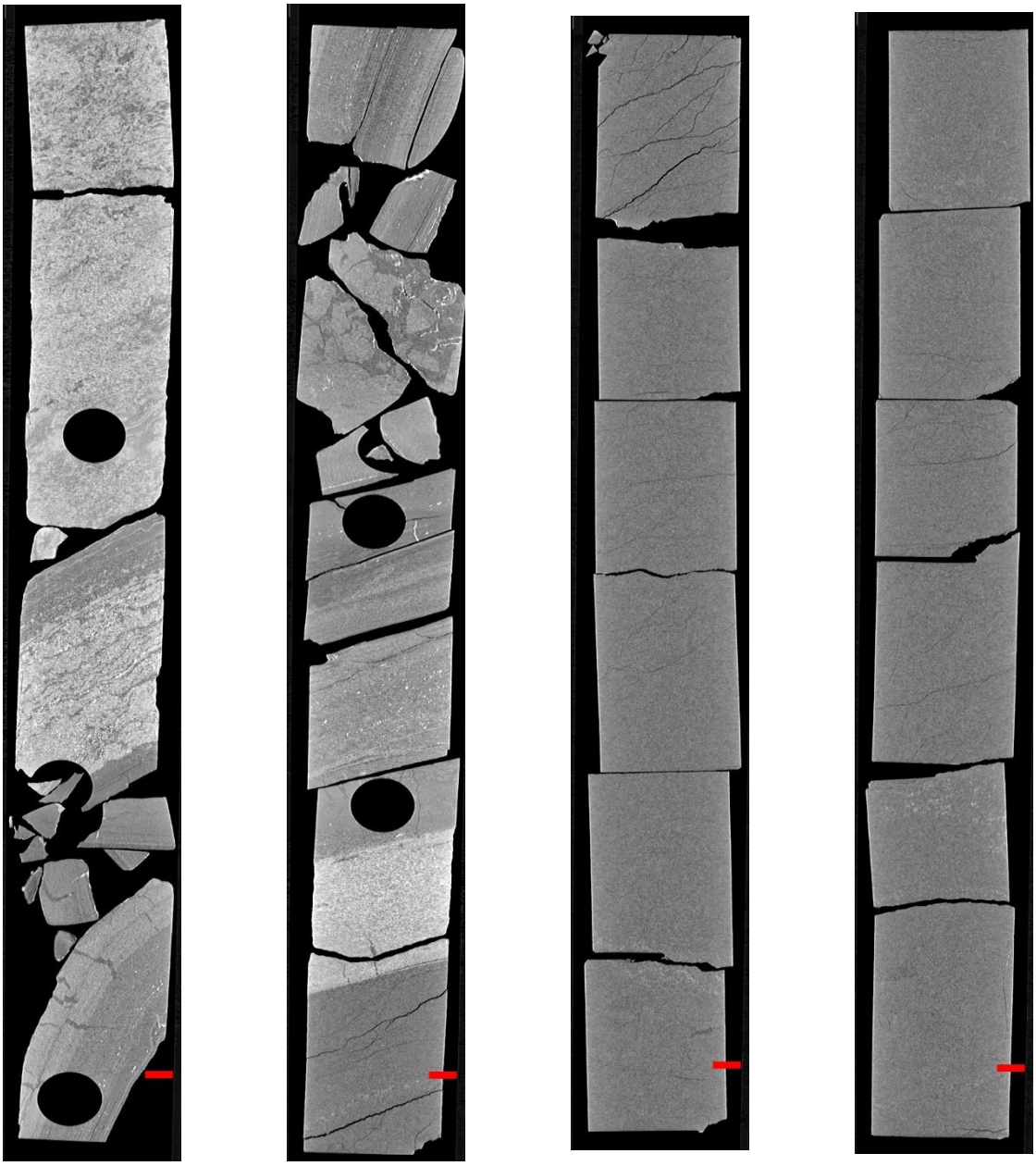

9,732–9,735 ft | 9,735–9,738 ft | 9,738–9,741 ft | 9,741–9,744 ft

**Figure 19: 2D isolated planes through the medical CT scans of the State 16-2 from 9,732 to 9,744 ft.**

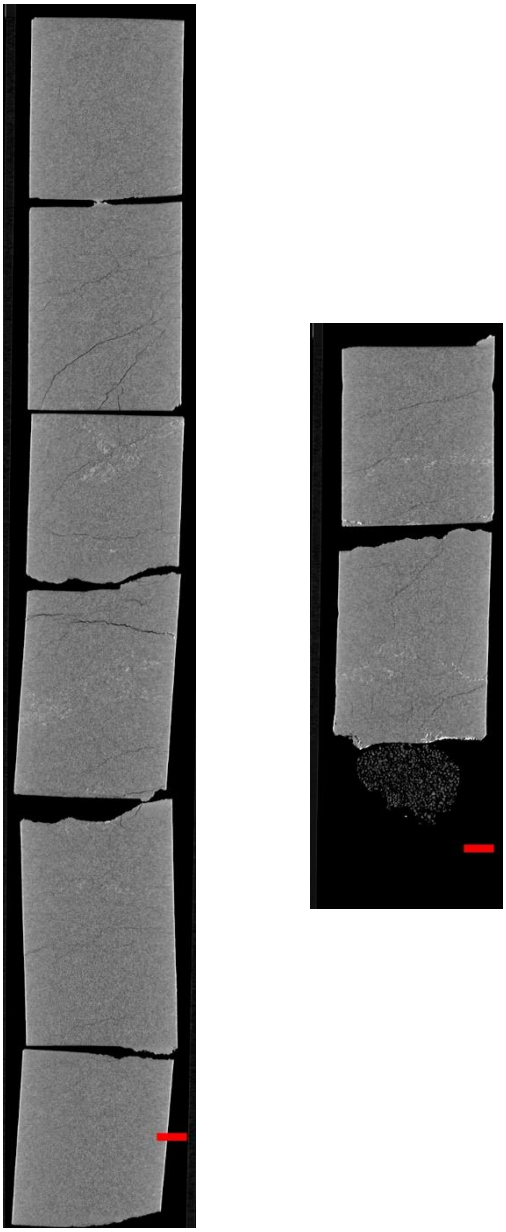

**9,744–9,747 ft** **9,747–9,748 ft**

**Figure 20: 2D isolated planes through the medical CT scans of the State 16-2 from 9,744 to 9,748 ft.**

## 4.2 ADDITIONAL CT DATA

Additional CT data can be accessed from NETL's EDX online system using the following link: https://edx.netl.doe.gov/dataset/paradox-state-16-2. The original CT data is available as 16-bit tif stacks suitable for use with ImageJ (Rasband, 2018) or other image analysis software. In addition, videos showing the variation along the length of the cross-section images shown in the previous section are available for download and viewing. A still image from these videos is shown in Figure 21. The red line through the XZ-plane image of the core shows the location of the XY-plane displayed above. The videos on EDX show this XY variation along the entire length of the core.

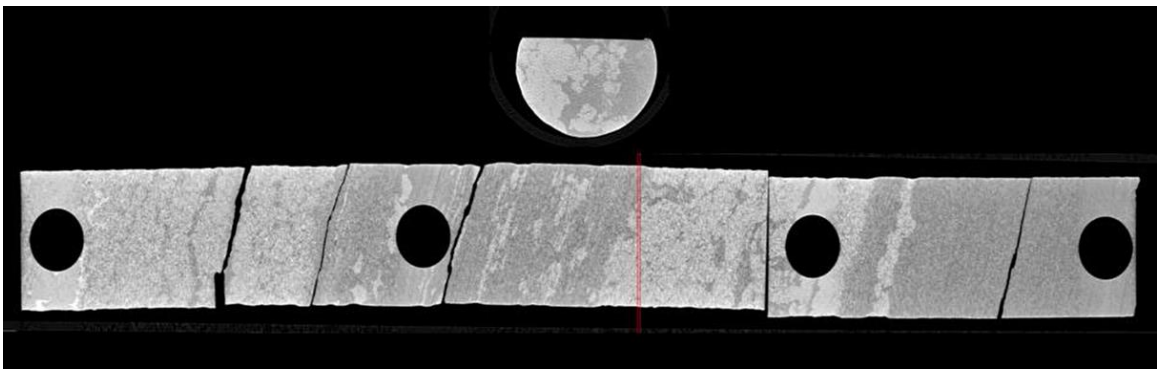

**Figure 21: Medical CT video of 9,699 to 9,702 representing a transition from dolomitic mudstone to anhydrite.**

### 4.2.1 Industrial CT Scanning

Detailed scans of sections of interest were performed with an Industrial CT scanner. The selected core sections are listed in Table 2 along with the voxel resolution and the image title on EDX. A montage image of "Paradox_9686 scan" is shown in Figure 22 as an example of the industrial CT images.

**Table 2: Industrial CT images from State 16-2 Well**

| Depth (ft) | Name | Voxel Resolution (µm³) |
|---|---|---|
| 9,686 | Paradox_9686 | 26.6 |
| 9,672 | Paradox_9672 | 52.3 |
| 9,700 | Paradox_9700 | 71.6 |
| 9,717 | Paradox_9717 | 45.9 |
| 9,737 | Paradox_9737 | 80.6 |

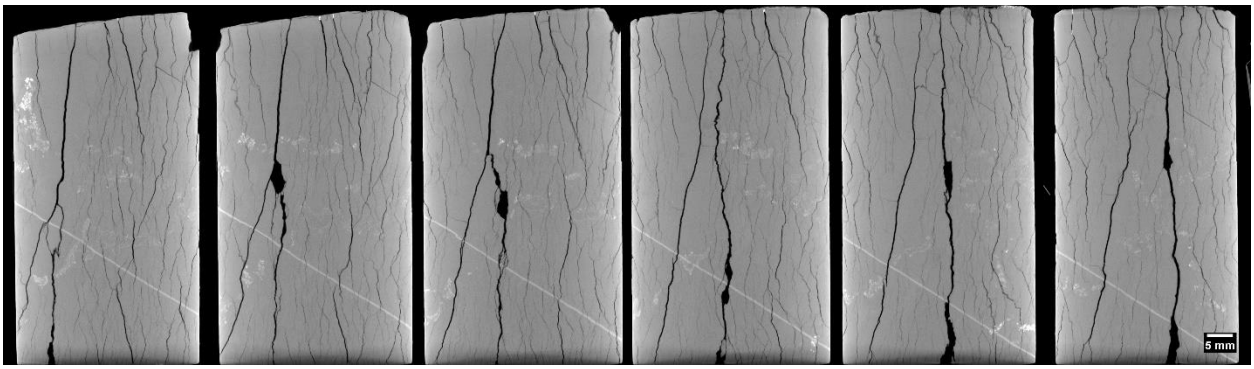


**Figure 22: State 16-2 industrial scan montage "Paradox_9686".**

### 4.2.2 Micro CT scanning

Detailed scans of section of interest were preformed using NETL's Dynatom and Xradia CT scanners. Table 3 and Table 4 list the selected intervals with depth and voxel resolution for each scanner. An example of the DynaTOM CT images are shown in Figure 19, where each image is an isolated slice along the length of the core (note each scale bar represents 0.5 cm).

**Table 3: Micro CT Images from the TESCAN DynaTOM**

| Depth | Name | Resolution |
|---|---|---|
| 9,639.3 | Paradox-Sample1.tif | 60.4 |
| 9,639.3 | Paradox-Sample1v2.tif | 60.4 |
| 9,648.15 | Paradox-Sample7.tif | 59.13 |
| 9,648.15 | Paradox-Sample7v2.tif | 59.13 |
| 9,656 | Paradox-Sample11.tif | 62.1 |
| 9,658.1 | Paradox-Sample12.tif | 50.8 |
| 9,661.1 | Paradox-Sample13.tif | 60.16 |
| 9,661.1 | Paradox-Sample13higher_res.tif | 32.5 |
| 9,661.1 | Paradox-Sample13v2.tif | 60.16 |
| 9,663.1 | Paradox-Sample14.tif | 60.6 |
| 9,664.4 | Paradox-Sample15.tif | 57.3 |
| 9,665.8 | Paradox-Sample17.tif | 61.4 |
| 9,670.1 | Paradox-Sample20.tif | 59.8 |
| 9,670.1 | Paradox-Sample20v2.tif | 59.8 |
| 9,670.1 | Paradox-Sample20v3.tif | 59.8 |
| 9,670.1 | Paradox-Sample20v4.tif | 59.8 |
| 9,679.25 | Paradox-Sample27.tif | 59.8 |
| 9,682.1 | Paradox-Sample28.tif | 59.8 |
| 9,693.1 | Paradox-Sample35.tif | 58.6 |
| 9,695.9 | Paradox-Sample37.tif | 57.1 |
| 9,703.9 | Paradox-Sample43.tif | 60.2 |
| 9,703.9 | Paradox-Sample43v2.tif | 60.2 |
| 9,705.1 | Paradox-Sample44.tif | 60.2 |
| 9,705.1 | Paradox-Sample44v2.tif | 60.2 |
| 9,710.1 | Paradox-Sample48.tif | 60.2 |
| 9,712.2 | Paradox-Sample49.tif | 60.2 |
| 9,719.05 | Paradox-Sample54.tif | 62.62 |
| 9,719.05 | Paradox-Sample54v2.tif | 62.62 |
| 9,726.1 | Paradox-Sample58.tif | 58 |
| 9,728.1 | Paradox-Sample60.tif | 61.4 |

**Table 4: Micro CT Images from the ZEISS Xradia MicroXCT-400 Scanner**

| Depth (ft) | Name | Voxel Resolution (µm³) |
|---|---|---|
| 9,672 | 20211008 Paradox Basin Emory C1B8 9672.0 | 4.02 |
| 9,672 | 20211015 Paradox Basin Emory C1B8 9672.0 sample 2 – 10x | 9.94 |
| 9,672 | 20211015 Paradox Basin Emory C1B8 9672.0 sample 2 – M70 | 4.02 |
| 9,734.2 | 20211020 Paradox Basin Emory C2B28 9734.2 – 10x | 9.94 |
| 9,734.2 | 20211015 Paradox Basin Emory C1B8 9734.2 – M70 | 4.02 |

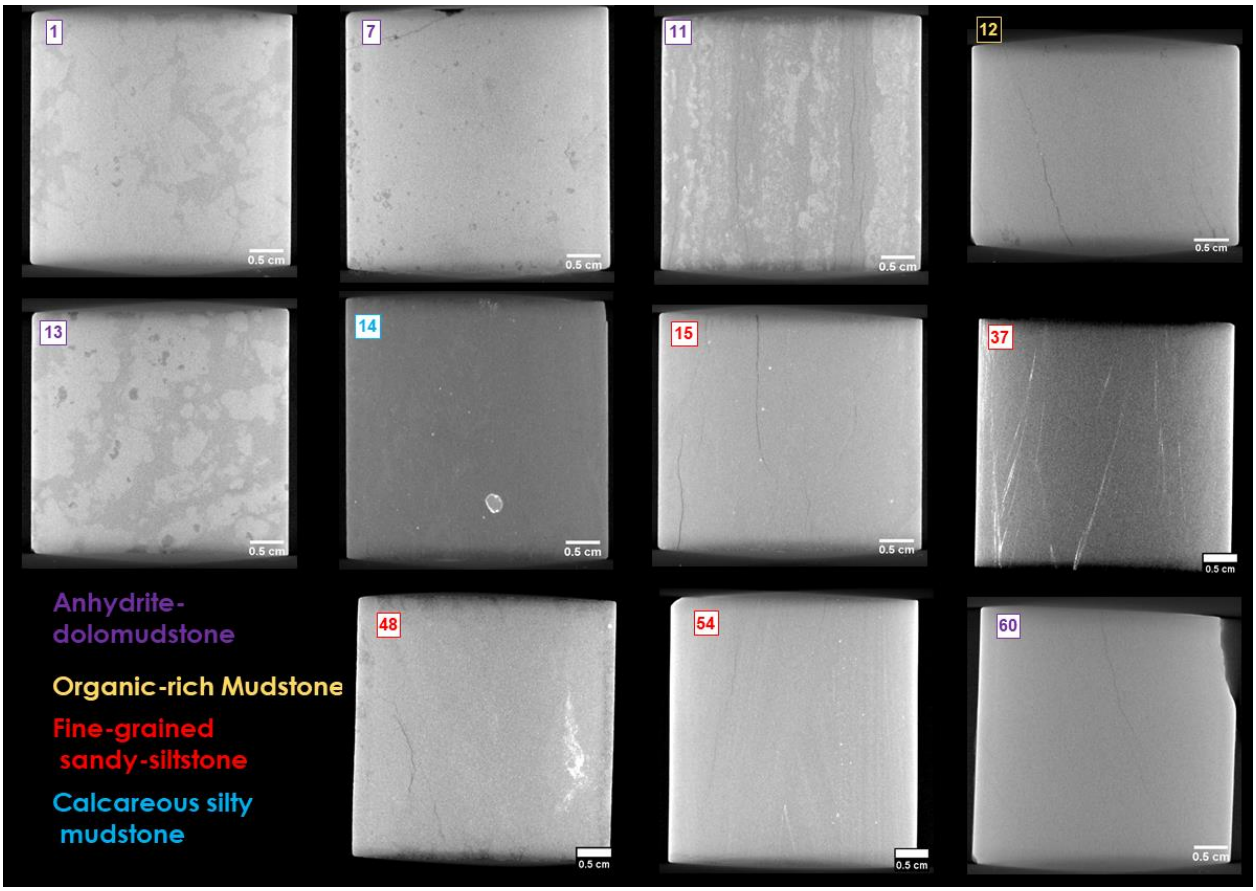


**Figure 23: Micro CT image reslices from the DynaTOM CT scanner. The numbers are related to the names in Table 3, color of label is related to lithology in the bottom left corner.**

## 4.3 PERMEABILITY MEASUREMENTS

Core scale permeability tests were performed on 12 subsamples selected from the State 16-2 well at increasing effective confining pressures (500 to 4,500 psi) using the RaSSCAL. Samples 1, 7, 11, 12, 13, 14, 15, 17, 20, 24, 37, 48, 53, 54, and 60 listed above in Table 3. The results shown in Figures 20 and 21 are separated by dominate lithology and sandy-siltstone, respectively. The raw data associated with these plots is available on EDX.

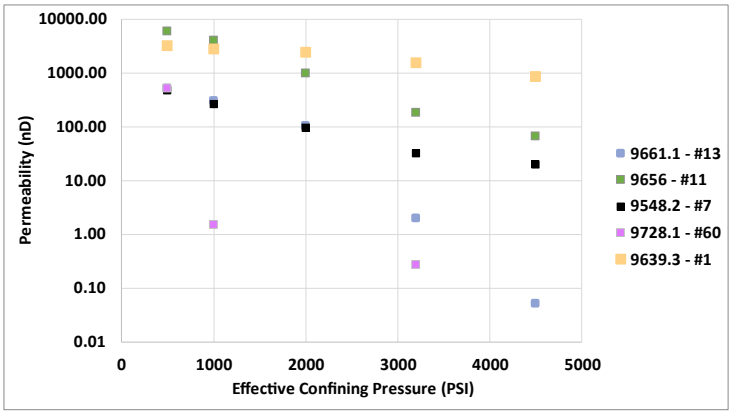


**Figure 24: Permeability vs. effective confining pressure for anhydrite-dolomudstone samples.**

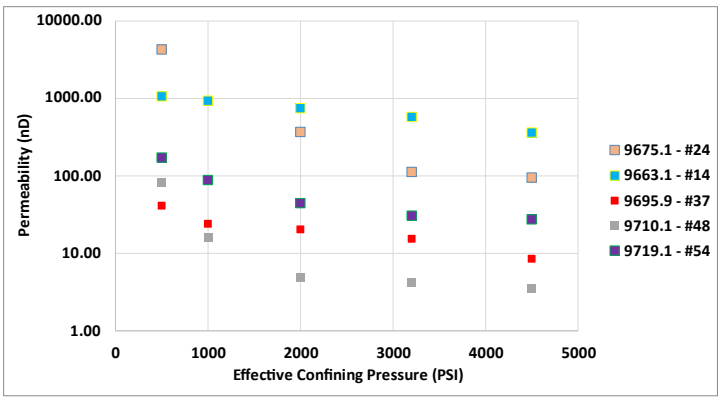


**Figure 25: Permeability vs. effective confining pressure for sandy-siltstone samples.**

## 4.4 COMPILED CORE LOG

The compiled core logs were scaled to fit on single pages for rapid review of the combined data from the medical CT and MSCL. Two sets of logs are presented in this section: the first set with data for the major elements and elemental ratios, and the second set with elemental proxies and CT image data. Features that can be derived from these combined analyses include determination of mineral locations, such as pyrite, from magnetic susceptibility. The XRF is used to inform geochemical composition and mineralogy.

Data from the MSCL was filtered to remove areas of fractures and missing core. The P-wave velocity was limited to values greater than 330 m/s as previously discussed. The gamma density, and medical CT derived dual energy density, were limited to values greater than 1.5 g/cm$^3$.

The elemental results from the XRF were limited to major elements (combined Light Elements, Ca, Si, Al) and elemental proxies related to redox potential (Cu and V), biogenic production (P and V*), skeletal influx/carbonate potential (Ca and Mn), detrital influence (Zr, Ti, Al, Si), and chalcophiles (Pb, S, Fe).

Trends in elemental ratios can provide insight into mineral composition, oxidation state, and depositional setting. Examples include: Ca/Si, which provides information on relative abundance of calcium carbonates versus silicates; Mn/Fe, which provides information on oxidation, where a decrease in the ratio is related to zones of anoxic/euxinic conditions and an increase is related to zones of dysoxic/oxic conditions; Ca/Mg, which provides information on dolomite; S/Fe, which provides information on the abundance of pyrite (and other iron sulfates) versus Fe oxide minerals; Fe/Al, which provides information about the degree of pyritization in shales; Ti/Al, which provides information about terrigenous input; and Si/Al, which provides information on the abundance of illite and micas versus other clays. Magnetic susceptibility can test for iron sulfides (reducing) or oxidized Fe and sulfate. The elemental proxy log also includes an XRF "mineralogy" with Al, representing clays; Ca, representing calcite; and Si, representing only quartz, although there is some Si contribution to the clays. Pyrite (reduced) should have low magnetic susceptibility, and Fe oxide or hydroxide should have high magnetic susceptibility. These broad trends can quickly give information on large suites of core and direct more focused research. These logs are presented in the following images.

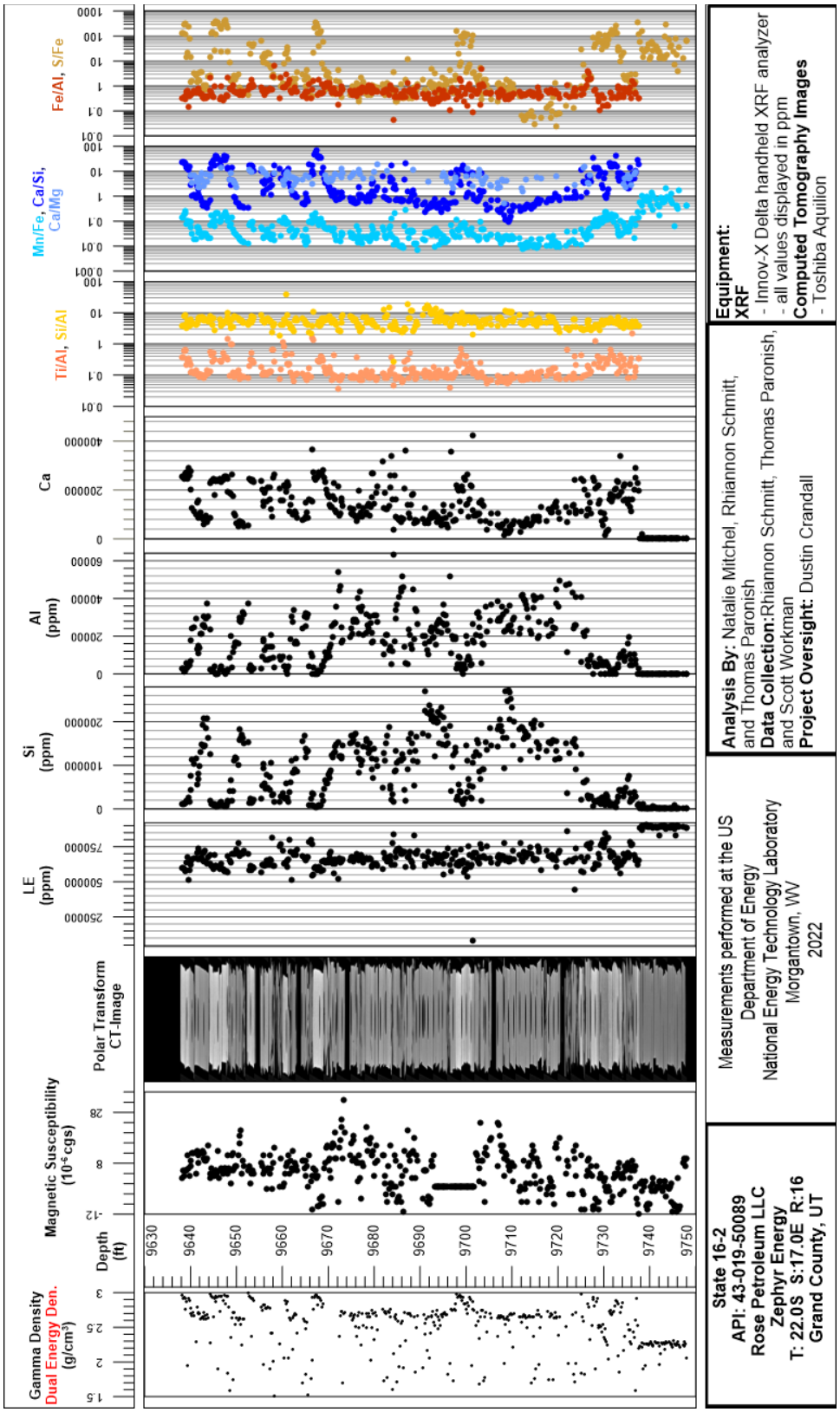


**Figure 26: Compiled core log of elemental ratios for the State 16-2 Well.**

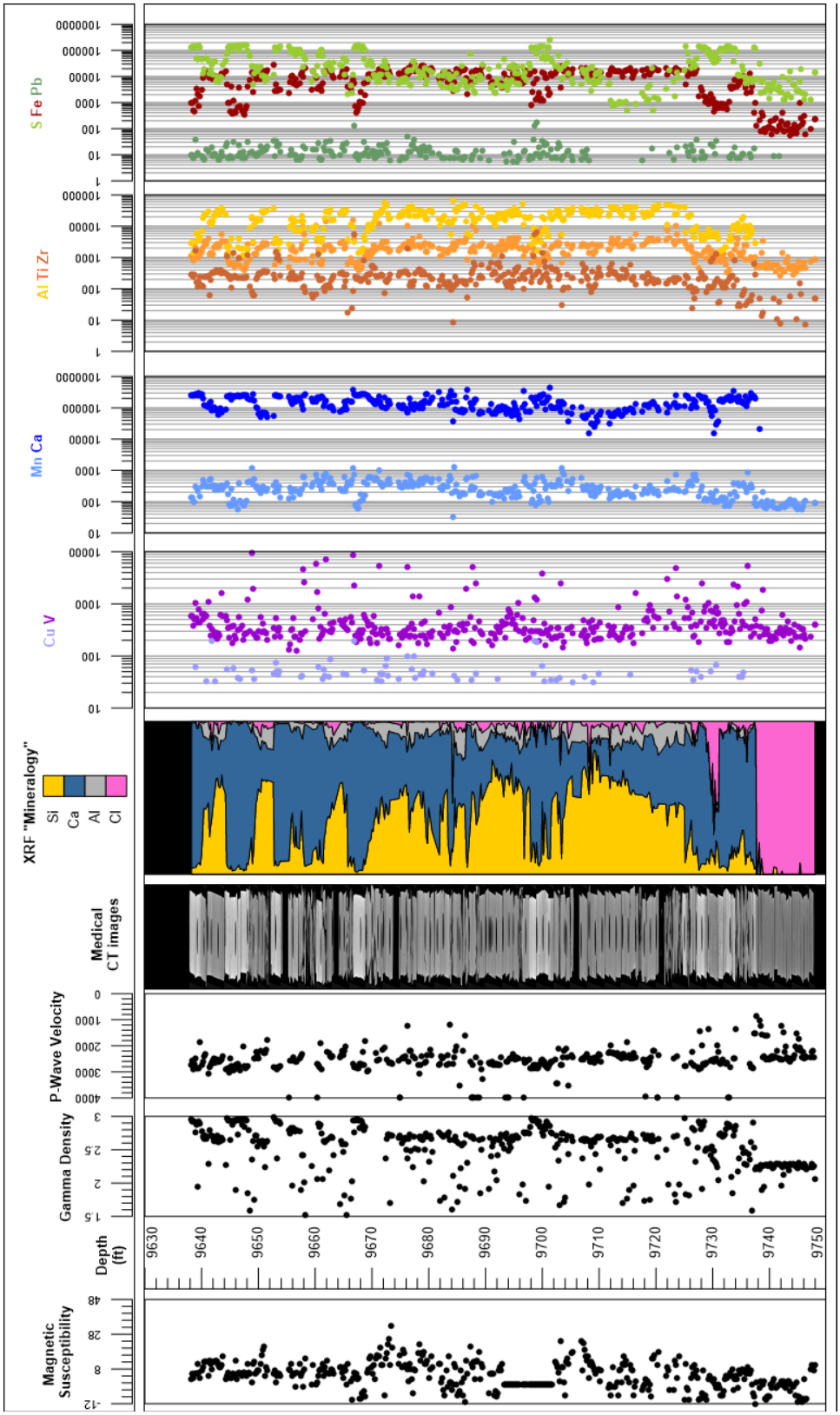


**Figure 27: Compiled core log with elemental proxies for the State 16-2 Well.**

## 5. DISCUSSION

The measurements of the magnetic susceptibility, gamma density, P-wave velocity, XRF, and CT analysis provide a unique look into of the internal structure of the core and macroscopic changes in lithology. These techniques:

- Are non-destructive
- When performed in parallel, give insight into the core beyond what one individual technique can provide
- Can be used to identify zones of interest for detailed analysis, experimentation, and quantification
- Provide a detailed digital record of the core, before any destructive testing or further degradation, that is accessible and can be referenced for future studies.

## 6. REFERENCES

Geotek Ltd. Multi-Sensor Core Logger Manual; Version 05-10; Published by Geotek, 3 Faraday Close, Daventry, Northamptonshire NN11 8RD, 2010. info@geotek.co.uk, www.geotek.co.uk

Hannon, M. J.; Tucker, Y. T.; Soeder, D. J. Quantifying the effects of gaseous pore pressure and net confining stress on low-permeability cores using the "RaSSCAL" steady-state permeameter. *Journal of Petroleum Science and Engineering* **2019,** *179*, 1136–1150.

Hunts, C.; Moskowitz, B.; Banerjee, S. *Magnetic Properties of Rocks and Minerals;* Rock Physics and Phase Relations: A Handbook of Physical Constants; 1995; p 189-204.

Paronish, T. J.; Crandall, D.; Moore, J. E.; Mckisic, T.; Michell, N.; Brown, S.; Tennant, B.; Workman, S.; Edelman, E.; McPherson, B.; Esser, R. *Core Characterization of the Cane Creek Interval in the Paradox Formation from the State 16-2 Well;* Rocky Mountain Section AAPG Conference; Denver, CO, 2022.

Rasband, W. S. ImageJ. U.S. National Institutes of Health: Bethesda, MD, 1997–2016, http://imagej.nih.gov/ij/ (accessed 2018).

Whidden, K. J.; Anna, L. O.; Pearson, K. M.; Lillis, P. G. *Assessment of Undiscovered Oil and Gas Resources in the Paradox Basin Province, Utah, Colorado, New Mexico, and Arizona;* United States Geological Survey Fact Sheet 2012-3031; 2012; p 4.

This page intentionally left blank.

**Brian Anderson**
Director
National Energy Technology Laboratory
U.S. Department of Energy

**David Alleman**
Associate Director
Office of Research & Development (FE-32)
U.S. Department of Energy

**John Wimer**
Acting Chief Research Officer
Science & Technology Strategic Plans & Programs
National Energy Technology Laboratory
U.S. Department of Energy

**Bryan Morreale**
Associate Laboratory Director for Research & Innovation
Research and Innovation Center
National Energy Technology Laboratory
U.S. Department of Energy